some kind of correspondence between this state and some state or states of Pb^{207}. The sum of the peak cross sections of the Pb^{207} states is 9.9 mb/sterad while the peak cross section of the 1.58-Mev state is 7.75 mb/sterad. The observed ratio of the two cross sections, including the experimental error, is 1.3 ± 0.4 and should be unity for corresponding states. The experimental data are therefore not in good agreement with this assumption of corresponding states. However, the discrepancies between the different experimental data do not appear to be sufficiently large to rule out the possible interpretation offered here.

(c) Comparisons with Other Experiments

The electron decay of Bi^{207} to the low-lying states of Pb^{207} has been studied by Alburger and Sunyar.[4] Our experimental angular distributions and relative cross sections for the ground state and first two excited states are in agreement with their configuration assignments.

An extensive survey of (d,p) and other reactions in several lead isotopes has been carried out by Harvey.[20] His Q-value and differential cross section measurements were carried out at a fixed angle. Several of our Q-value measurements appear to disagree with his results although the combined uncertainties are large enough to account for the discrepancies. On the basis of his relative cross sections for the different states (at one laboratory angle) and using the j-j coupling scheme by Klinkenberg,[19] Harvey assigned single-particle or single-hole configurations to all of his observed states in Pb^{207} and Pb^{209}. In particular, his assignments for the 2.71-Mev, 3.61-Mev, 4.37-Mev, and 4.62-Mev states of Pb^{207} were $g_{9/2}$, $i_{11/2}$, $d_{5/2}$, and $g_{7/2}$. His assignments for the ground, 0.79-Mev, and 1.58-Mev states of Pb^{209} were $g_{9/2}$, $i_{11/2}$, and $d_{5/2}$, and the possible correspondence of these states with states in Pb^{207} was pointed out. Our experimental results indicate that the 0.79-Mev state of Pb^{209} does not correspond to the 3.61-Mev state of Pb^{207}. Furthermore, our experimental results do not seem to permit simple unmixed configuration assignments for the 4.37-Mev and 4.62-Mev states of Pb^{207}. A possible interpretation of this doublet and its relation to the Pb^{209} 1.58-Mev state has been offered.

[20] J. A. Harvey, Can. J. Phys. **31**, 278 (1953).

ACKNOWLEDGMENTS

We gratefully acknowledge the advice and assistance in the interpretation of these measurements offered to us by Professor K. W. Ford, Dr. W. W. True, and Professor E. J. Konopinski. We wish also to express our appreciation to Mr. Sam Polley for his assistance in the operation of the cyclotron.

PHYSICAL REVIEW VOLUME 111, NUMBER 6 SEPTEMBER 15, 1958

Electrodisintegration of Be^9 and C^{12}†

W. C. BARBER
High-Energy Physics Laboratory, Stanford University, Stanford, California
(Received March 31, 1958)

Yields from the reactions $Be^9(e,e'n)$ and $Be^9(\gamma,n)$, as well as the relative yields from $C^{12}(e,e'n)C^{11}$ and $C^{12}(\gamma,n)C^{11}$, were measured under conditions which permitted a comparison of the relative effects of electrons and bremsstrahlen from electrons in producing nuclear reactions. The primary electron energies were from 6 to 17 Mev in the case of Be, and 24 to 145 Mev in the case of C. Comparison of the experimental results with the theory of electrodisintegration gives information about the multipole order of the electromagnetic transitions involved. The Be^9 results agree with theory if the reaction mechanism is predominantly electric-dipole. For C^{12}, a mixture of 92% electric-dipole with 8% electric-quadrupole intensities gives agreement with theory over the energy range 28–145 Mev, provided that the finite size of the C nucleus is taken into account. The method of considering the finite nuclear size in the theory is presented, and the results previously obtained by Reagan for the reactions $F^{19}(e,e'2p)N^{17}$ and $F^{19}(\gamma,2p)N^{17}$ are shown to be in good agreement with the modified theory for an electric-quadrupole transition.

I. INTRODUCTION

THE direct interaction of the electromagnetic field of an electron with the nuclear charges and currents is closely related to the interaction of photons with the nucleus. One important difference arises from the fact that when a nucleus absorbs the energy of a photon, the momentum transfer is fixed along the direction of the incident photon; whereas in transferring energy to the nucleus the electron scatters, giving rise to a distribution of momentum transfers. To the approximation that the nuclear size can be neglected, the relative effects of photons and electrons in producing nuclear reactions can be evaluated without knowledge of the nuclear wave functions other than the specification of the multipole order of the

† Supported by the joint program of the Office of Naval Research, the U. S. Atomic Energy Commission, and the U. S. Air Force Office of Scientific Research.

nuclear transition involved. Specification of the multipole order is required because this determines the angular distribution of the scattered electrons and hence the distribution of momentum transfers. It is noteworthy that in case the electron energy is just above the threshold for the reaction under study, the scattered electron has almost no energy, and hence the momentum transfer is very nearly in the initial electron direction. If, in addition, the initial electron energy is large compared with its rest energy, the energy and momentum transfer relations are essentially the same as for a photon; and a comparison of photo- and electrodisintegration cross sections no longer gives information about the multipole order of the nuclear transition.

Calculations of the ratio of photo- to electrodisintegration cross sections, approximating the nucleus as a point and the incoming and outgoing electrons as plane waves, have been made by a number of investigators.[1–3] Similar calculations for an energy domain where the finite nuclear size cannot be neglected have been made by Dalitz and Yennie.[4]

Various experiments comparing photo- and electrodisintegration cross sections have been reported. The most recent of those concerned with nuclear excitations below meson threshold are those of Brown and Wilson[5]; Scott, Hanson, and Kerst[6]; Reagan[7]; and Hines.[8] Brown and Wilson studied reactions resulting in the ejection of a single neutron from Cu^{63}, Zn^{64}, Ag^{109}, and Ta^{181}, using primary electrons of energies from 24 to 35 Mev. In the cases of Cu, Zn, and Ag, their results were in agreement with theory provided the transitions involved were approximately 88% electric-dipole and 12% electric-quadrupole. In the case of Ta a considerably larger fraction of quadrupole transitions was required to give agreement between experiment and theory. The authors favored an alternate explanation: that the approximations of the theory were not sufficiently accurate for a high-Z nucleus such as Ta. Hines[8] extended the measurements on Cu^{63} to primary electron energies of 81 Mev and also studied the ejection of three neutrons from Mn^{55} producing 21-min Mn^{52}. Hines remarked that the finite nuclear size would be expected to modify the theory at these high bombarding energies but he did not attempt a quantitative evaluation of these effects. Reagan's work was also at higher energies where nuclear size should not be neglected.

The present work on Be^9 and C^{12} was undertaken to compare theory and experiment in the low-Z region where the plane-wave approximation should be most nearly valid. The work on C^{12} was extended to energies high enough that finite nuclear size effects should become important. A rough evaluation of these effects has been made using the work of Dalitz and Yennie[4] as a basis. The finite nuclear size has a particularly strong influence on the excitation of electric-quadrupole transitions by electrons. This is illustrated by a comparison of Reagan's results on the production of N^{17} from F^{19} with the size-corrected theory.

II. EXPERIMENTAL METHOD

The required experimental data are the measured yields of neutrons or radioactivities produced when electrons of known energy E_0 bombard thin targets, and the corresponding yields when the bremsstrahlen from electrons of energy E_0 bombard similar targets.

In practice it was convenient to obtain the ratio of these yields by employing foil sandwiches as electron targets in the method used by Brown and Wilson.[5] For the carbon experiments the sandwich consisted of a thin polystyrene sheet, then a tantalum radiator, followed by a second polystyrene sheet. The entire sandwich was "thin" so that almost the entire electron beam traversed the sandwich with little loss in energy. Under these circumstances the activity $N_1(E_0)$ induced in the first target foil was almost entirely due to electrons, while that in the second target $N_2(E_0)$ was the sum of activities induced by electrons and the bremsstrahlen produced in the radiator. Since the target foils were of equal thickness, the quantity $(N_2-N_1)/N_1$ gives approximately the ratio of photon- to electron-induced activity. In practice the foil stack could not be thin enough to use this equation directly, and corrections to take account of foil thickness were required.

In the appendix these corrections are listed, and it is shown that to first order in the foil thickness, the correct ratio of photon- to electron-induced activities is given by

$$R(E_0-\tfrac{1}{2}\Delta_t)=R'\left\{1-R'\left[\frac{\frac{1}{2}t_t+t_f}{t_t+t_r}\right]\right\}^{-1}, \qquad (1)$$

where

$$R'=\left[N_2(1-\tfrac{1}{2}\langle\theta^2\rangle)+\frac{\partial(N_1+N_2)}{\partial E_0}\frac{(\Delta_t+\Delta_r)}{2}-N_1\right]N_1^{-1}. \qquad (2)$$

All symbols are defined in the appendix.

For the Be^9 experiment where the reaction was detected by counting neutrons, the foil-stack experiment was modified and performed in two stages. In one case, the electron beam bombarded a target of $\frac{1}{8}$-in. beryllium, and in the second case, the target was a sandwich consisting of a $\frac{1}{16}$-in. aluminum radiator followed by a $\frac{1}{8}$-in. beryllium target. The primary electron beam was monitored by a hydrogen-filled ionization chamber placed ahead of the target. Backgrounds for the respective experiments were obtained by employing as targets either an empty target holder

[1] G. C. Wick, Ricerca sci. **11**, 49 (1940).
[2] J. S. Blair, Phys. Rev. **75**, 907 (1949).
[3] Thie, Mullin, and Guth, Phys. Rev. **87**, 962 (1952).
[4] R. H. Dalitz and D. R. Yennie, Phys. Rev. **105**, 1598 (1957).
[5] K. L. Brown and R. Wilson, Phys. Rev. **93**, 443 (1954).
[6] Scott, Hanson, and Kerst, Phys. Rev. **100**, 209 (1955).
[7] D. Reagan, Phys. Rev. **100**, 113 (1955).
[8] R. L. Hines, Phys. Rev. **105**, 1534 (1957).

or the aluminum radiator only. (Onset of copious production of neutrons from the aluminum radiator limited the primary beam energies to 18 Mev.) The net yield from the beryllium target was predominantly due to the direct electrodisintegration, while the net yield from the (Al+Be) sandwich was due to the photons produced in the aluminum radiators as well as to direct electrodisintegration.

Analysis of the data to give the corrected ratio of photo- to electrodisintegration yields is similar to the process described for the three-foil radioactivity experiments, and is described in further detail in the appendix.

III. EXPERIMENTAL DETAILS

Because the electrodisintegration cross sections are $\sim 1/137$ times the photodisintegration cross sections, the experiment requires knowledge of any photon contamination of the primary electron beam. This was achieved through use of the double magnetic deflecting systems of the Mark III and Mark II electron linear accelerators.[9,10] In these systems the electron beam is deflected and refocused after it has been collimated and energy-analyzed, so that the bremsstrahlung produced in collimators and energy-defining slits is not traveling in the final direction of the electrons. The purity of the final electron beam was established by studying beam pictures on photographic film or glass plates, and by the good reproducibility of the ratio of photo- to electrodisintegration observed in the present experiments. (Any photon contamination of the beam would be expected to vary with accelerator tune-up conditions which produce changes in the electron spot size and energy spectrum.) The reaction yields due to unknown photon contamination of the incident beam were estimated to be less than 1% of the electron-induced activity in the present experiments.

In the case of the C^{12} experiments using the Mark II accelerator, the foil stacks were placed inside the accelerator vacuum system, so no correction for radiation-producing material ahead of the targets was required. In the other experiments, where some material was unavoidably directly in front of the targets, a small correction was required (see appendix).

The energy calibration of the Mark II accelerator was established to 2% accuracy by measurements of the thresholds of the reactions $D(\gamma,n)$, $Cu^{63}(\gamma,n)$, and $O^{16}(\gamma,n)$. The energy calibration of the Mark III accelerator was taken from floating-wire measurements made on the deflecting magnets.

The detectors for the 20-min C^{11} were anthracene scintillation counters. A pair of counters was employed so that the front and back detector foils could be counted simultaneously. Successive counting periods were made interchanging foils on the counters so that possible differences in counting efficiencies could be observed and taken into account. Successive bombardments were made in which front and rear detector foils were interchanged so that small variations in detector foil thickness were averaged out.

The neutrons from the Be^9 reaction were detected by BF_3 counters enriched in B^{10} which were embedded in paraffin moderator surrounding the target. This neutron counting assembly was constructed and calibrated by W. D. George for use in an experiment to measure absolute neutron yields from various targets. Construction and calibration details will be published later. For the present experiment, where only the ratio of yields (with and without radiator) was desired, the efficiency calibration of the counters was not important. A source of error lies in the possibility that the neutrons from the electrodisintegration and from the photodisintegration have different angular distributions. However, the moderator surrounded the targets except for openings in the forward and backward directions, and measurements with a RaBe source indicated that 78% of the total solid angle was sampled. An estimate of the possible error due to angular distribution effects can be obtained from the data of Hamermesh *et al.*[11] on the angular distribution of neutrons from the $Be^9(\gamma,n)$ reaction. They observed a distribution of the form $(a+b\sin^2\theta)$ where $a/b \gg 1$ near threshold and $a/b=1.2$ at $h\nu=2.76$ Mev. If we take $a/b=1.2$ for the photodisintegration process and $a/b=\infty$ (isotropic) for the electrodisintegration process, the computed efficiency for photon-produced relative to electron-produced neutrons is 1.015. From the theoretical considerations mentioned in the introduction, we expect the electron-produced neutrons to have a distribution somewhat more isotropic than but similar to that of the photoproduced neutrons. Thus the ratio 1.015 computed on the assumption of isotropy for the electron-produced neutrons is an upper limit to the error from this source.

The hydrogen-filled ionization chamber used to monitor the incident electron beam in the Be^9 experiments was used in a previous experiment on the specific ionization of electrons in gases.[12] Its reproducibility at given energy was within 1%, and its sensitivity as a function of electron energy was known to 1% accuracy over the energy range employed.

IV. THEORY

The results of the theories can be expressed in terms of a spectrum of virtual photons, associated with an electron of initial energy E_0, available for producing nuclear excitations of energy k_f and of specified multipole order. (We use units throughout such that $\hbar=c=1$.)

For a point nucleus the matrix elements for electron-induced transitions can be expressed in terms of those for photon-induced transitions, and the electrodisinte-

[9] W. K. H. Panofsky and J. A. McIntyre, Rev. Sci. Instr. **25**, 287 (1954).
[10] K. L. Brown, Rev. Sci. Instr. **27**, 959 (1956).
[11] Hamermesh, Hamermesh, and Wattenberg, Phys. Rev. **76**, 611 (1949).
[12] W. C. Barber, Phys. Rev. **97**, 1071 (1955).

gration cross section can be written

$$\sigma_e(E_0,k_f,l)=\frac{N_e}{k_f}(k_f,E_0,l)\sigma_\gamma(k_f), \tag{3}$$

where N_e is the virtual photon intensity spectrum associated with a transition energy k_f and multipole order specified by l, and $\sigma_\gamma(k_f)$ is the cross section for photons of energy k_f. The theoretical calculations give the result

$$N_e\frac{dk_f}{k_f}=\frac{\alpha}{\pi}\frac{dk_f}{k_f}\left\{\left[1+\left(\frac{E_0-k_f}{E_0}\right)^2\right]\times\ln\frac{2E_0(E_0-k_f)}{m_0k_f}-C\right\}, \tag{4}$$

where m_0 is the rest energy of the electron, $C\equiv 2(E_0-k_f)/E_0$ for electric-dipole transitions, $C\equiv 0$ for magnetic-dipole transitions, and $C\equiv-(8/3)[(E_0-k_f)/k_f]^2$ for electric-quadrupole transitions. Thie, Mullin, and Guth[3] show how the calculations can be extended to higher orders, give an explicit result for electric-octupole transitions, and stress the uncertainty of the magnetic-multipole calculations because of the unknown nature of the mesonic contributions to the magnetic moments.

Dalitz and Yennie[4] have extended the calculations to the region where the nuclear size is no longer small in comparison with the length associated with the momentum transferred to the nucleus. In their paper N_e is separated into contributions $N_e{}^t$ and $N_e{}^l$ from those parts of the matrix elements transverse and longitudinal to the direction of the momentum transfer. Their result [Eq. (1.5) of reference 4] is

$$N_e(p,k_f)=N_e{}^t(p,k_f)+N_e{}^l(p,k_f), \tag{5}$$

where

$$N_e{}^t(p,k_f)=\frac{\alpha}{\pi}\int_{(p-p')^2}^{(p+p')^2}\frac{k_f{}^2d(k^2)}{(k_0{}^2-k^2)^2}\times\left\{\frac{[(p+p')^2-k^2][k^2-(p-p')^2]}{4p^2k^2}+\frac{k^2-k_0{}^2}{2p^2}\right\}\frac{\langle J_t{}^2(k^2)\rangle}{\langle J_t{}^2(k_f{}^2)\rangle}, \tag{6}$$

and

$$N_e{}^l(p,k_f)=\frac{\alpha}{\pi}\int_{(p-p')^2}^{(p+p')^2}\frac{k_f{}^2d(k^2)}{4k_0{}^2p^2}\times\left[\frac{(p+p')^2}{k^2}-1\right]\frac{\langle J_t{}^2(k^2)\rangle}{\langle J_t{}^2(k_f{}^2)\rangle}. \tag{7}$$

The new symbols employed here are defined as follows: p and p' are the magnitudes of the electron's momentum before and after scattering; k_0 and k are the energy and magnitude of the momentum transferred to the nucleus; $\langle J_t{}^2\rangle$ and $\langle J_l{}^2\rangle$ are the squares of those parts of the matrix element transverse and longitudinal to the direction of the momentum transfer. For a point nucleus the matrix element components have the values shown in Table I. Integration of Eqs. (5), (6), and (7), with the values from Table I inserted and with the extreme relativistic approximation that $E_0=p$, results in Eq. (4).

TABLE I. Values of the ratios of the matrix elements for transitions of various multipole order when the nucleus is treated as a point.

Type of transition	$\frac{\langle J_t{}^2(k^2)\rangle}{\langle J_t{}^2(k_f{}^2)\rangle}$	$\frac{\langle J_l{}^2(k^2)\rangle}{\langle J_t{}^2(k_f{}^2)\rangle}$
$E1$	1	1
$M1$	$k^2/k_f{}^2$	0
$E2$	$k^2/k_f{}^2$	$+\frac{4}{3}(k^2/k_f{}^2)$

An exact calculation of the matrix element ratios for the case where the nuclear size is not negligible would require knowledge of the initial and final state wave functions. However, an estimate of the effect of the finite nuclear size can be obtained by assuming that contributions to the matrix elements occur uniformly throughout the nuclear volume. At each point $\mathbf{r}$ the contribution to the matrix element should contain the phase factor $e^{i\mathbf{k}\cdot\mathbf{r}}$, so that the corrected expression for the matrix elements would have the form

$$J_{\text{finite}}(k)=\int\psi_f{}^*[\text{operator}]e^{i\mathbf{k}\cdot\mathbf{r}}\psi_i d\tau. \tag{8}$$

In order to integrate (8) over the nuclear volume, the phase factor is expanded as usual in spherical Bessel functions and Legendre polynomials:

$$e^{i\mathbf{k}\cdot\mathbf{r}}=\sum_l(2l+1)i^l j_l(kr)p_l(\cos\theta)=1-\tfrac{1}{6}k^2r^2+\cdots. \tag{9}$$

The evaluation of (8) to lowest order in kr gives an expression for the matrix elements of a finite-size nucleus in terms of those for a point nucleus:

$$J_{\text{finite}}(k)=J_0(k)[1-\tfrac{1}{6}\langle r^2\rangle]. \tag{10}$$

The ratios for the squares of the matrix elements that appear in Table I should be multiplied by the factor

$$\frac{[1-\frac{1}{6}k^2\langle r^2\rangle]^2}{[1-\frac{1}{6}k_f{}^2\langle r^2\rangle]^2}\approx\frac{1-\frac{1}{3}k^2\langle r^2\rangle}{1-\frac{1}{3}k_f{}^2\langle r^2\rangle} \tag{11}$$

before substitutions into Eqs. (6) and (7). Integration of (6) and (7) then yields values of N_e for producing excitation of a nucleus of finite size. The calculation could easily be carried to higher-order approximation, but in view of the uncertainty in ψ_i and ψ_f this is not warranted at this time.

Since the principal contributions to $N_e{}^t$ occur for values of k approximately equal to k_f, it is not changed much by the effect of finite nuclear size. However, the principal contribution to $N_e{}^l$ comes from larger values

TABLE II. Experimental data for the Be^9 reactions. Target, 0.589 g/cm² Be; $t_t=8.67\times10^{-3}$. Radiator, 0.4362 g/cm² Al; $t_r=1.79\times10^{-2}$. Material ahead of foil stack, $t_f=3.6\times10^{-4}$. $F_{exp}=[Z(Z+1)r_0^2N_r]^{-1}R=7.104R$.

E_0 (Mev)	N_1	N_2	$1-\frac{1}{2}\langle\theta^2\rangle$	Δ_r (Mev)	Δ_t (Mev)	$\frac{\partial N_2}{\partial E_0}\left(\frac{\Delta_r-\Delta_t}{2}\right)$	$\frac{\partial N_1}{\partial E_0}\left(\frac{\Delta_r+\Delta_t}{2}\right)$	R''	$R(E_0-\frac{1}{2}\Delta_t)$	$E_0-\frac{1}{2}\Delta_t$ (Mev)	$F_{exp}(E_0-\frac{1}{2}\Delta_t)$
5.5	1028±27	1888±23	0.96	0.76	0.94	−53	280±28	0.984±0.05	1.328±0.08	5.03	9.444±0.57
7.9	1929±36	3623±33	0.98	0.81	0.98	−63	285±28	0.955±0.035	1.275±0.06	7.41	9.06 ±0.45
10.3	2837±68	5408±45	0.99	0.85	0.99	−53	360±36	0.995±0.04	1.348±0.07	9.80	9.58 ±0.51
12.7	3935±27	7249±35	0.993	0.90	1.02	−45	402±40	0.920±0.019	1.214±0.040	12.19	8.63 ±0.31
15.1	4715±22	8630±21	0.995	0.94	1.04	−31	326±33	0.884±0.011	1.151±0.037	14.58	8.18 ±0.26
17.5	5422±32	10 073±41	0.996	0.99	1.07	−18	267±27	0.896±0.013	1.173±0.039	16.97	8.33 ±0.27

TABLE III. Experimental data for the C^{12} reaction. Targets, 0.077 g/cm² polystyrene; $t_t=1.68\times10^{-3}$. Radiator, 0.172 g/cm² Ta; $t_r=2.71\times10^{-2}$. (Correction for Z dependence of bremsstrahlung from radiator, 1.07±0.007.) $F_{exp}=(4.097\pm0.027)R$.

E_0 (Mev)	N_2/N_1	t_f	$1-\frac{1}{2}\langle\theta^2\rangle$	$\frac{(\Delta_t+\Delta_r)}{2}$ (Mev)	$\frac{1}{N_1}\frac{\partial(N_1+N_2)}{\partial E_0}\times\frac{(\Delta_t+\Delta_r)}{2}$	R'	$R(E_0-\frac{1}{2}\Delta_t)$	$E_0-\frac{1}{2}\Delta_t$ (Mev)	$F_{exp}(E_0-\frac{1}{2}\Delta_t)$
23.5	2.679±0.03	0	0.99	0.465	0.806±0.08	2.457±0.085	2.647±0.095	23.4	10.85±0.40
27.1	2.982±0.03	0	0.993	0.511	0.305±0.03	2.264±0.042	2.424±0.066	27.0	9.93±0.27
30.5	2.948±0.03	0	0.994	0.558	0.176±0.02	2.107±0.036	2.245±0.040	30.4	9.20±0.18
33.6	2.894±0.03	0	0.995	0.597	0.092±0.01	1.972±0.031	2.092±0.035	33.5	8.57±0.16
36.0	2.885±0.03	0	0.996	0.643	0.028±0.003	1.901±0.03	2.013±0.035	35.9	8.25±0.16
40.0	2.755±0.03	8.2×10^{-4}	0.997	0.688	0.010±0.001	1.735±0.03	1.928±0.039	39.9	7.90±0.16
75.7	2.261±0.03	19.5×10^{-4}	1.00	1.273	0.006±0.000	1.268±0.03	1.446±0.045	75.5	5.92±0.19
140.0	2.087±0.03	19.5×10^{-4}	1.00	2.197	0.008±0.000	1.097±0.03	1.228±0.044	139.8	5.03±0.18

of k, and the factor (11) produces a substantial reduction. For large values of k the factor $1-\frac{1}{3}k^2\langle r^2\rangle$ becomes negative. This is a result of the approximation and cannot represent a real physical situation; hence the integrals of the modified Eqs. (6) and (7) have been taken only over the region where the integrand is positive.

In all the calculations it was assumed that $\langle r^2\rangle$, the mean square nuclear radius, is given by $[1.2\times10^{-13}A^{\frac{1}{3}}]^2$.

V. RESULTS AND COMPARISON WITH THEORY

The principal experimental results, together with data on the targets and radiators, are presented in Tables II and III. The final errors quoted are statistical combinations of various errors from the sources listed in the tables. The errors introduced by the correction terms were estimated to be 10% of the applied correction. The correction and analysis of the results requires knowledge of the activation curves $N_1(E_0)$ and $N_2(E_0)$. In the case of beryllium the determination of these activation curves was a part of the experiment. Figure 1 shows activation curves for the electron- and photon-induced reactions in Be. These curves are the quantities $N_e(E_0)-N_\gamma(E_0)$ after correction as indicated in the appendix. The photodisintegration cross section as determined from the photon-difference analysis of the photon activation curve is shown as the histogram in Fig. 2. For comparison, the cross-section curve determined by Nathans and Halpern[13] is shown by the dashed line. The curves were arbitrarily normalized to contain approximately equal areas. Although the errors in the present experiment preclude any detailed comparison of the cross sections in the region beyond 6 Mev, the relatively high value of the cross section obtained in the present experiments at ~3 Mev is in good agreement with experiments performed with monochromatic γ rays in this energy region.

For the present C^{12} experiments only the relative

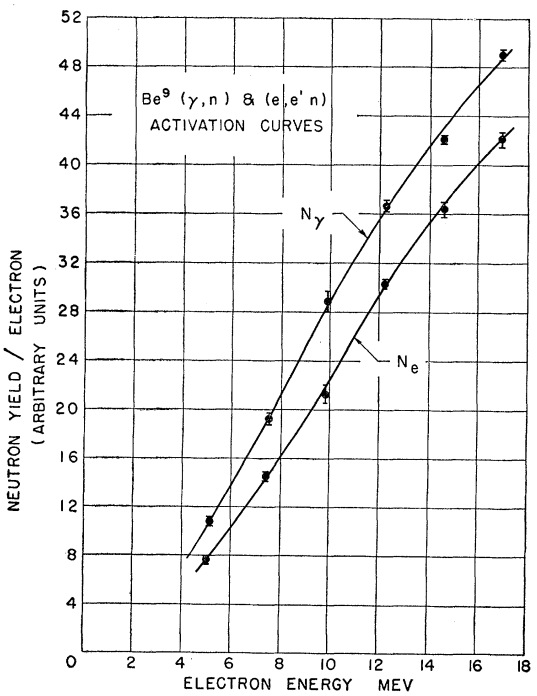

FIG. 1. Activation curves for the photo- and electrodisintegration of Be^9.

[13] R. Nathans and J. Halpern, Phys. Rev. **92**, 940 (1953).

values of N_1 and N_2 were measured. Using these ratios, activation curves $N_1(E_0)$ and $N_2(E_0)$ were determined from the results of Barber, George, and Reagan[14] where the activation and cross-section curves for the reaction $C^{12}(\gamma,n)C^{11}$ were determined.

Finally available from experiment are the corrected ratios [Eq. (1)] giving the relative yields of a reaction from the bremsstrahlen and the direct effect of an electron of energy E_0. The theory is able to predict this ratio for a process with a fixed value of the transition energy k_f and a given multipole order. Since both the reactions under study have a cross section which is significant over a wide range of k_f, it is necessary to average the theoretical predictions over k_f before a comparison with experiment can be made. The theoretical ratio to be compared with experiment is

$$N_r\int_0^{E_0}\sigma(k_f)\varphi_\gamma(E_0,k_f,Z)\frac{dk_f}{k_f}\Big/\int_0^{E_0}\sigma(k_f)N_e(E_0,k_f)\frac{dk_f}{k_f}, \tag{12}$$

where N_e is given by Eq. (4) or (5), φ_γ is the bremsstrahlung intensity spectrum produced by an electron of energy E_0 in the radiator of atomic number Z, and N_r is the effective number of atoms/cm^2 in the radiator. In the present work, the Bethe-Heitler formula with intermediate screening is used as the basis for φ_γ. Screening is neglected in computing N_e because here the principal contributions come from "close" collisions, the same fact that makes nuclear-size effects so important. Consideration must be given to the bremsstrahlung produced in the field of the atomic electrons of the radiator and to the fact that for high atomic numbers the Bethe-Heitler formula overestimates the amount of radiation produced. A sufficiently accurate correction for the former effect is obtained by applying the factor $(Z+1)/Z$ to the radiation formula. For the latter effect an empirically determined correction factor for the Z dependence of bremsstrahlung[15] is used. As a matter of convenience, these corrections have been made to the experimental ratio (1) rather than to (12). Since N_e depends on the multipole order of the transition, Eq. (12) should be written separately for each multipole transition using for $\sigma(k_f)$ that part of σ which is due to the multipole order under consideration. In practice we have little direct knowledge of the multipole order of the processes producing the reactions under study, and we expect a comparison of experiment and theory to tell us something about this. For a first-order comparison we have computed values of Eq. (12) under the assumption that the process is of a single multipole order over the entire range of k_f. Figures 3 and 4 show a comparison of the ratios computed from Eq. (12) by numerical integration and the experimentally determined ratios Eq. (1) as functions of E_0. In order to permit a comparison with the convention of Blair[2] employed by Brown and Wilson[5] and others, both ratios (12) and (1) were multiplied by the constant quantity $(Z^2r_0^2N_r)^{-1}$ before they were plotted. Multiplication by this factor removes the experimental quantity N_r from the theoretical ratio and gives

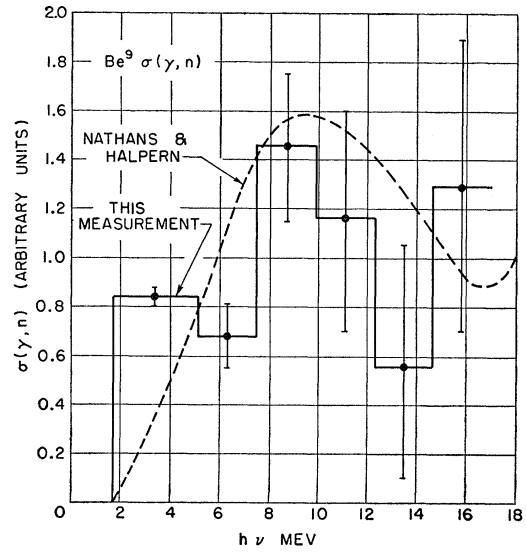

FIG. 2. Cross-section curves for the reaction $Be^9(\gamma,n)$. The histogram is the cross section derived by photon difference analysis of the photon activation curve shown in Fig. 1. The dashed curve is the cross section as determined by Nathans and Halpern.[13]

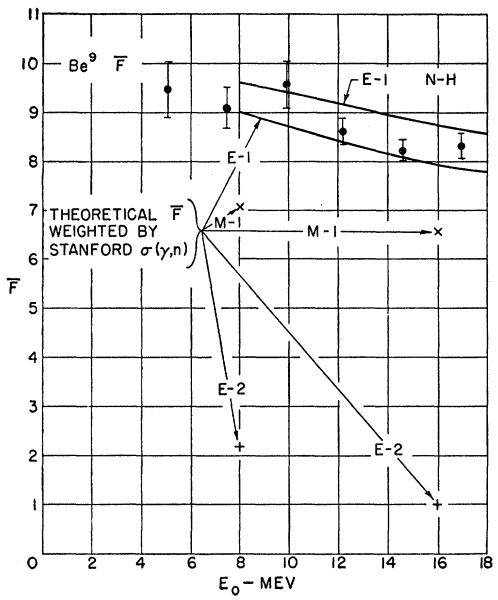

FIG. 3. Ratio of the yields of neutrons from Be^9 by photodisintegration to those by electrodisintegration, as a function of primary electron energy. The experimental ratios are indicated by points with standard errors shown. Theoretical ratios calculated under different assumptions are indicated by the arrows.

[14] Barber, George, and Reagan, Phys. Rev. **98**, 73 (1955).

[15] Barber, Berman, Brown, and George, Phys. Rev. **99**, 59 (1955).

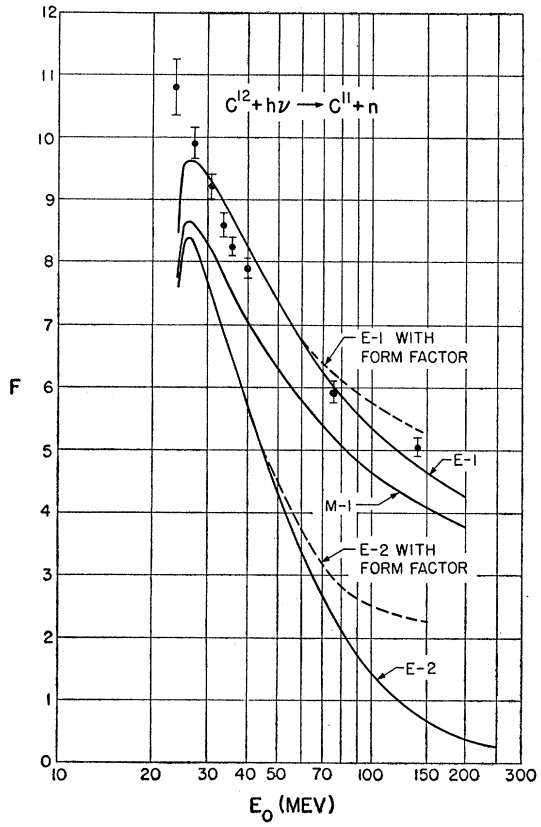

FIG. 4. Ratio of the yields of C^{11} from the photodisintegration of C^{12} to those from the electrodisintegration, as a function of primary electron energy. Experimental ratios are shown as points with standard errors. The theoretical ratios assuming a point nucleus are shown as solid curves. The dashed curves are for a nucleus of finite size.

directly the ratio F defined by Blair[2] and employed by Brown and Wilson,[5] and Reagan.[7] The results for Be^9 and C^{12} are shown in Figs. 3 and 4 with the experimental ratios as plotted points and the theoretical ratios as curves. Reagan's experimental values of the ratio F for $F^{19} \rightarrow 2p+N^{17}$ are shown in Fig. 5. Since Reagan found that the activation curve for the reaction was indistinguishable from an isochromat with $k_f=40$ Mev, the theoretical ratios have been computed by using a delta function at $k_f=40$ Mev for $\sigma(k_f)$ in Eq. (12).

A. Be^9

Figure 3 indicates that the experimental results are in very good agreement with the theory if the reaction is almost entirely electric-dipole. There are two theoretical electric-dipole curves shown in Fig. 3 corresponding to the two cross-section curves of Fig. 2. The difference in the two curves for F comes chiefly from the difference in the cross-section curves at low energies, and is relatively insensitive to the other differences. The lower theoretical curve for F which was derived from the present measurements is better for comparison with the experimental F values for two reasons: (1) any error in the determination of the cross-section curve due to variation of counter efficiency with neutron energy would cancel in the determination of F; (2) the high cross section at a photon energy of about 3 Mev observed in the present experiments is checked independently by experiments using monoenergetic γ-rays. The agreement between experiment and electric-dipole theory is in accord with the model of Guth and Mullin[16] for the photodisintegration of Be^9. It should be noted, however, that the experiment is not very sensitive in discriminating between electric- and magnetic-dipole transitions, and a fractional intensity of 10 or 20% of magnetic-dipole transition cannot be ruled out.

B. C^{12}

The experimental points fall fairly close to the theoretical curves for electric-dipole absorption. The point at 24 Mev apparently disagrees with theory. Part of this disagreement might be related to the finite end point of the bremsstrahlung spectrum, which has been neglected in the present analysis. However, it should be pointed out that 24 Mev is very near the peak of the cross-section curve and the corrections for thick-target effects are large and uncertain. It is believed that the present experiment is not an adequate test of the theory in this region. As the energy is increased the experimental points fall below the electric-dipole curve. The experimental uncertainties decrease as the energy is increased, and the data give evidence for participation of magnetic-dipole or more likely electric-quadrupole transitions. Independent evidence for a mixture of transitions

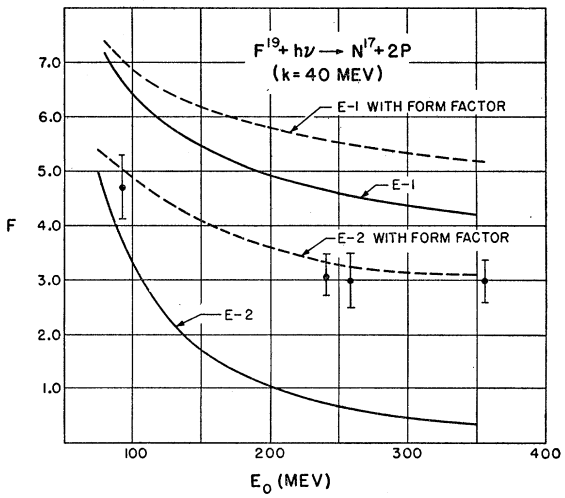

FIG. 5. Ratio of the yields of N^{17} from the photodisintegration of F^{19} to those from the electrodisintegration, as a function of primary electron energy. The experimental ratios are shown as points with standard errors. The theoretical ratios assuming a point nucleus are shown as solid curves. The dashed curves are for a nucleus of finite size.

[16] E. Guth and C. J. Mullin, Phys. Rev. **76**, 234 (1949).

is supplied by the experiments of Dodge and Barber[17] which show a $\cos\theta$ term in the angular distribution of photoprotons from C^{12}. A quadrupole intensity of about 8% would give agreement with both experiments. The points at 75 and 145 Mev lie on and above the theoretical electric-dipole curve for a point nucleus. This would be in disagreement with the evidence for a mixture of other types of transitions. However, if the finite-nuclear-size effects are included, the theoretical F values are shifted up as shown by the dashed curves in Fig. 4, and the comparison of experiment and theory remains compatible with an electric-quadrupole intensity of a few percent.

C. $F^{19} \rightarrow 2p + N^{17}$

The F values and their standard deviations as determined by Reagan do not fit with any mixture of transitions if only the theories for a point nucleus are considered. The point at 90 Mev suggests a large amount of electric-quadrupole intensity whereas the higher-energy points do not support this. The photon activation curve is like an isochromat at $k_f = 40$ Mev, and therefore it is not possible to make a reconciliation by assuming new electric-dipole processes which come in at higher values of k_f. However, when the theory is corrected for the finite size of the nucleus the experimental points fall along the theoretical electric-quadrupole curve. This result suggests that the $F^{19} \rightarrow 2p + N^{17}$ reaction is a direct process with the two protons emitted in opposite directions or at least with some symmetry relation such that the dipole matrix elements are nearly zero.

D. Conclusion

The comparison of the present experiments on Be^9 and C^{12} with the electrodisintegration theories gives results in very good accord with present ideas about the photodisintegration of these nuclei. The theory of the electrodisintegration of low-Z nuclei is thus checked within experimental error. The results for $F^{19} \rightarrow 2p + N^{17}$ indicate how experiments of this type are a very sensitive test for the occurrence of electric-quadrupole transitions, and if the experiments were performed with high precision they could provide data on the nuclear form factors for these transitions.

VI. ACKNOWLEDGMENTS

The writer wishes to thank Professor D. R. Yennie for most helpful discussion and explanation of the effects of nuclear size in electrodisintegration experiments. Thanks are also due Dr. Burton Richter for providing convenient space and opportunity for bombarding C^{12} in his experimental setup on the Stanford Mark III accelerator.

[17] W. R. Dodge and W. C. Barber, Bull. Am. Phys. Soc. Ser. II, 2, 377 (1957).

APPENDIX. CORRECTIONS FOR THE FINITE THICKNESS OF THE TARGET AND RADIATOR FOILS

The following processes must be taken into account in analyzing the stacked-foil experiments: (a) reduction of the electron energy as the foil stack is traversed; (b) effective loss of electrons through radiation and collision in the foil stack; (c) change in the effective thickness of the foils due to multiple scattering of the electrons; (d) radiator thickness effects in the production of bremsstrahlung; (e) activity induced in the target foils by the bremsstrahlung produced in the target foils themselves; (f) any activity due to bremsstrahlung produced in the region "upstream" from the foil stack.

A. Definition of Symbols

E_0 = energy of incident electrons.
$N_1(E_0)$ = activity (or yield) per electron induced in the first target foil.
$N_2(E_0)$ = activity (or yield per electron induced in the second target foil, the target foil that is behind the radiator.
t_t = target thickness in radiation lengths.
t_r = radiator thickness in radiation lengths.
t_f = total material upstream from the foil stack in radiation lengths.
Δ_t = total electron energy loss in the target by radiation and collision.
Δ_r = total electron energy loss in the radiator by radiation and collision.
$\langle\theta^2\rangle$ = mean square scattering angle of the electrons in the radiator (scattering in the targets can be neglected).
N_γ = that part of N_2 due to photons produced in the first target and the radiator.
N_e = that part of N_1 due to the direct effect of electrons.
$R' = N_\gamma/N_1$ in the three-foil stack experiments.
$R'' = N_\gamma/N_1$ in the two-stage experiments.
$R = N_\gamma/N_e$.

B. Calculation of the Corrections

First consider experiments of the C^{12} type where a three-foil stack (target 1/radiator/target 2) is employed. The quantity

$$N_\gamma(E_0 - \Delta_t - \tfrac{1}{2}\Delta_r) = N_2(1 - \tfrac{1}{2}\langle\theta^2\rangle) + \frac{\partial N_1}{\partial E_0}(\Delta_t + \Delta_r) - N_1 \quad \text{(A-1)}$$

gives the photon-induced activity in the second target due to the bremsstrahlen coming from the first target and the radiator. N_1 and N_2 contain equal activities from photons produced ahead of the foil stack and from photons produced by the target foils acting as their own radiator; hence these effects cancel in Eq. (A-1).

The term in $\langle\theta^2\rangle$ corrects for the fact that both the radiator and the second target are effectively thicker due to multiple scattering in the radiator. The term containing $\partial N_1/\partial E_0$ corrects for the fact that the electron-induced effect in foil 2 is less than in foil 1 because of effects (a) and (b). [Corrections for these effects could be made separately by dividing the electron energy loss into two categories: small energy losses that reduce the electron's effectiveness, and large energy losses which substantially remove the electron from the beam. Of these the former is more important; and it is sufficiently accurate to take the latter type into account by writing the total energy loss in the correction term for effect (a).] Effect (d) involves many processes which can be taken into account in detail.[18] For the present work it was sufficiently accurate to approximate the thick-target bremsstrahlung spectrum produced by electrons of energy E_0 by the thin-target spectrum produced by electrons at the mean energy in the radiator $E_0-\Delta_t-\frac{1}{2}\Delta_r$. Equation (A-1) is then interpreted as the photo-effect due to bremsstrahlung by electrons of this reduced energy. Since N_1 is produced by electrons of mean energy $E_0-\frac{1}{2}\Delta_t$, it is necessary to increase Eq. (A-1) by

$$\frac{\partial(N_2-N_1)}{\partial E_0}\left(\frac{\Delta_t+\Delta_r}{2}\right)$$

in order to have a photoeffect corresponding to an energy $E_0-(\Delta_t/2)$ for comparison with N_1. This yields

$$N_\gamma(E_0-\tfrac{1}{2}\Delta_t)=N_2(1-\tfrac{1}{2}\langle\theta^2\rangle)+\frac{\partial(N_1+N_2)}{\partial E_0}\left(\frac{\Delta_t+\Delta_r}{2}\right)-N_1, \quad \text{(A-2)}$$

which when divided by N_1 is the R' given in Eq. (2). It remains to correct for effects (e) and (f). Since these effects subtracted away in Eq. (A-1), it is necessary only to correct N_1 in the denominator of Eq. (2).

[18] R. Wilson, Proc. Phys. Soc. (London) **A66**, 683 (1953).

Effect (e) produces the same activity as a radiator of thickness $\frac{1}{2}t_t$. Effect (f) is due to a thickness t_f. $N_\gamma[E_0-\frac{1}{2}\Delta_t]$ represents the activity due to an actual radiator of thickness (t_r+t_t). Therefore, N_1 must be reduced to obtain

$$N_e(E_0-\tfrac{1}{2}\Delta_t)=N_1-N_\gamma(E_0-\tfrac{1}{2}\Delta_t)\left[\frac{\frac{1}{2}t_t+t_f}{t_r+t_t}\right], \quad \text{(A-3)}$$

the yield due to the direct effect by electrons only. Division of Eq. (A-2) by (A-3) results in Eq. (1).

When the experiment is performed in two stages, as was the case for Be^9, the analysis is basically the same, but because of the fact that target 1 is absent while the yield from target 2 is being measured, the results are different. In this case,

$$N_\gamma(E_0-\tfrac{1}{2}\Delta_r)=N_2(1-\tfrac{1}{2}\langle\theta^2\rangle)+\left(\frac{\partial N_1}{\partial E_0}\times\Delta_r\right)-N_1. \quad \text{(A-4)}$$

To obtain $N_\gamma[E_0-(\Delta_t/2)]$ corresponding with N_1, we must add to (A-4) the quantity

$$\frac{\partial(N_2-N_1)}{\partial E_0}\left(\frac{\Delta_r-\Delta_t}{2}\right).$$

This gives

$$N_\gamma(E_0-\tfrac{1}{2}\Delta_t)=N_2(1-\tfrac{1}{2}\langle\theta^2\rangle)-N_1+\frac{\partial N_2}{\partial E_0}\left(\frac{\Delta_r-\Delta_t}{2}\right)+\frac{\partial N_1}{\partial E_0}\left(\frac{\Delta_r+\Delta_t}{2}\right). \quad \text{(A-5)}$$

Corrections for effects (e) and (f) are exactly the same as in the three-foil experiment. The corrected ratio of photon- to electron-induced activity is

$$R(E_0-\tfrac{1}{2}\Delta_t)=R''\Big/\left\{1-R''\left[\frac{\frac{1}{2}t_t+t_f}{t_r}\right]\right\}, \quad \text{(A-6)}$$

where

$$R''=\frac{N_\gamma(E_0-\frac{1}{2}\Delta_t)}{N_1}. \quad \text{(A-7)}$$